Reversible Switching of Strong Light–Matter Coupling Using Spin-Crossover Molecular Materials

Lijun Zhang, Karl Ridier, Oleksandr Ye. Horniichuk, Stéphane Calvez, Lionel Salmon, Gábor Molnár, Azzedine Bousseksou

Reversible Switching of the Strong Light-Matter Coupling Using Spin-Crossover Molecular Materials

Lijun Zhang, Karl Ridier*, Oleksandr Ye. Horniichuk, Stéphane Calvez, Lionel Salmon, Gábor Molnár, and Azzedine Bousseksou*

Lijun Zhang, **Karl Ridier**, **Oleksandr Ye. Horniichuk**, **Lionel Salmon**, **Gábor Molnár**, **Azzedine Bousseksou**
Laboratoire de Chimie de Coordination, CNRS UPR 8241, Université de Toulouse
205 route de Narbonne, F-31077 Toulouse, France
Email: karl.ridier@lcc-toulouse.fr; azzedine.bousseksou@lcc-toulouse.fr

Stéphane Calvez
Laboratoire d'Analyse et d'Architecture des Systèmes, CNRS UPR 8001, Université de Toulouse
7 avenue du colonel Roche, F-31400 Toulouse, France

Abstract

The formation of hybrid light-matter states, through the resonant interaction of confined electromagnetic fields with matter excitations, has emerged as a fascinating tool for controlling quantum-mechanical states and then manipulating functionalities and chemical reactivity landscape of molecular materials. Here, we report the first observation of switchable strong light-matter coupling involving bistable spin-crossover molecules. Spectroscopic measurements, supported by transfer-matrix and coupled-oscillator simulations, reveal Rabi-splitting values up to 550 meV, which at 15 % of the molecular excitation energy enters the regime of ultrastrong coupling. We find that the thermally induced switching of molecules between their low-spin and high-spin states allows a fine control of the light-matter hybridization strength, offering the appealing possibility of a reversible switching between ultrastrong and weak coupling regimes within a single photonic structure. Through this work, we show that spin-crossover molecular compounds constitute a promising class of active nanomaterials in the burgeoning context of tunable polaritonic devices and polaritonic chemistry.

TOC Graphic

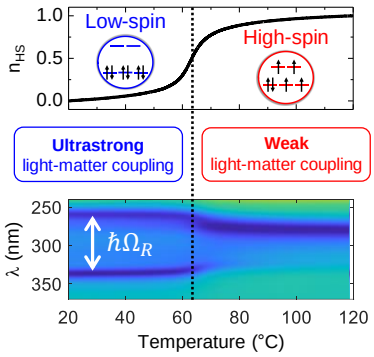

The field of polaritonic chemistry, wherein molecular systems are studied under the regime of strong light-matter coupling, has become the topic of intense experimental and theoretical research over the past decade.[1–6] This field aims at manipulating chemical structures and reactions (aspiring to achieve novel molecular functionalities), through the formation of hybrid light-matter states between organic molecules and confined electromagnetic (EM) modes in optical nano-/micro-cavities. This regime of strong coupling can be achieved by placing an ensemble of molecules in a resonant photonic structure or an optical cavity (e.g. Fabry-Pérot cavities, plasmonic structures, etc.), designed such that one of the cavity modes is resonant with a molecular (electronic[7,8] or vibrational[9,10]) excitation, resulting in a coherent, oscillatory exchange of energy between the cavity and the material. Especially, if this energy exchange becomes faster than any competing dissipation (e.g. cavity-photon leakage) or decoherence (e.g. molecular dephasing) processes, then the so-called strong-coupling regime arises between the molecules and the surrounding EM field. In this case, new hybrid light-matter states (with mixed molecular and photonic character) – known as polaritons – are formed, with an energy separation, called Rabi-splitting energy ($\hbar\Omega_R$), being proportional to the coupling strength. An appealing feature is that this light-matter hybridization can occur even in the absence of real/applied photons inside the cavity, the coupling arising from the vacuum fluctuations, i.e., from the finite zero-point energy of the quantized EM field in the cavity.[1,6]

In that regard, organic molecular systems are of particular interest because exceptionally large vacuum Rabi-splitting energies (hundreds of meV)[8] can be achieved due to their large transition dipole moments (i.e. large absorption extinction coefficients) and high possible density of integration in the cavity. This allows the (ultra-)strong coupling regime to be achieved in relatively low quality-factor cavities ($Q \approx 10$).[8,11] In this context, the field of polaritonic chemistry is burgeoning both in interest and importance as it provides a fascinating tool to tune the energy landscape of the coupled system and modify the physico-chemical properties of molecules.[1–6] In particular, strong light-matter coupling between cavity photon modes and excitons in organic molecules has been used, for example, to change excited-state relaxation pathways,[12] chemical reactivity[10,13–15] or even charge and energy transport phenomena.[16] Within this field, the use of switchable, stimuli-responsive molecules as active materials is of great interest as it opens up appealing perspectives to reversibly activate/deactivate the strong-coupling regime in a single photonic cavity and, more generally, to explore the synergetic effects that can exist between light-matter hybridization and molecular bistability. Examples of strong-coupling regime involving switchable materials have been mostly reported so far with photochromic molecules (especially spiropyrans),[8,13,17–21] as well as a few phase-change materials,[22–24] providing prospects for active tuning and dynamical device reconfiguration.

In this article, we demonstrate that spin-crossover (SCO) molecules constitute an attractive class of stimuli-responsive materials that can be strongly coupled to optical cavity modes, to form switchable hybrid light-matter states. Indeed, these molecular coordination complexes can switch reversibly between the so-called low-spin (LS) and high-spin (HS) electronic configurations (see Figure 1a)

through the application of a variety of external perturbations, including a temperature change, the application of pressure, of an intense magnetic field, or by light irradiation.[25–27] Especially, the switching of the molecular spin state is known to involve a drastic change of the optical properties of the material (absorption coefficient and refractive index), which can be effectively harnessed for active photonic applications.[28–31] In this view, in a recent work,[31] we have demonstrated the fabrication of SCO-based Fabry-Pérot cavities displaying spectrally tunable resonances in the visible range (where the compound used is virtually transparent in both spin states) in response to the refractive index change of the SCO thin film upon the spin transition. A similar effect was also evidenced in plasmonic structures with embedded SCO thin films or particles.[29,32–34] However, the regime of strong light-matter interaction between switchable SCO molecules and resonant optical structures has never been studied so far.

Here, we report the observation of a light-matter hybridization between photon modes of purposefully-designed optical resonators and electronic excitations of SCO molecules, the latter exhibiting intense absorption bands in their LS form in the ultraviolet (UV) spectral domain. An ultrastrong coupling regime is evidenced with Rabi-splitting energies as large as 550 meV. As molecules in their HS state are transparent in this spectral domain, we show that the coupling strength can be fine-tuned (until reaching a weak-coupling regime) in a single photonic structure, via the thermally induced conversion of the molecules into the HS state. An interesting feature of SCO compounds is that the thermal transition between the LS and HS states can take various characteristics, from very gradual conversions over a wide temperature range, to abrupt transitions, with or without thermal hysteresis loop.[25] Therefore, in this work, through the investigation of two different SCO complexes, we demonstrate that the thermally induced switching between strong and weak coupling regimes can be achieved either gradually or abruptly, depending on the specific characteristics of the thermal spin transition, thus allowing either continuous tuning or ON/OFF switching of the Rabi splitting.

The studied samples consist of a thin layer of aluminum (16 nm), coated on the hypotenuse face of a fused-silica right-angle prism (which serves as a coupling medium), above which is deposited a film of a SCO complex (see Figure 1b). These Al/SCO bilayer structures indeed exhibit both transverse electric (s) and transverse magnetic (p) resonance modes, which can be excited under wavevector matching conditions using a coupling prism in the Kretschmann geometry. Two bilayer resonators were prepared using two different Fe^{2+} SCO molecular complexes. The first (hereafter denoted as resonator **1**) was coated with a layer of 153 nm of the complex [Fe(HB(1,2,3-triazol-1-yl)$_3$)$_2$] **1**,[35] while the second sample (denoted as resonator **2**) was prepared with a 138-nm-thick film of the complex [Fe(HB(1,2,4-triazol-1-yl)$_3$)$_2$] **2**.[36] These two isomeric compounds, which only differ by the position of an exodentate nitrogen atom in the triazolyl ring (see their molecular structures in the insets of Figures 1c and 1d, respectively), undergo spin transition above room temperature and have the property of being sublimable, i.e. they can be deposited by vacuum thermal evaporation in the form of high-quality, homogeneous thin films.[37,38] The optical absorbance spectra of the films of **1** and **2**, deposited on fused-silica substrates, exhibit intense, SCO-dependent absorption bands in the UV spectral range (Figure 1c

and 1d). More specifically, at room temperature (in the LS state), compound **1** displays two distinct, well-separated absorption peaks at 337 and 274 nm, while complex **2** exhibits three bands around 317, 305 and 272 nm. Taking into account the high absorption coefficients associated with these peaks (*ca.* 10^4 cm^{-1}), they presumably correspond to charge-transfer (metal-to-ligand and/or ligand-to-metal) transitions. It may be worth noting that these complexes also display Laporte-forbidden ligand-field transitions in the visible-NIR spectral domain, with absorption coefficients about 100 times lower (*ca.* 10^2 cm^{-1}),[39] which thus remain virtually undetectable in such nanometric thin films. As shown in Figures 1c and 1d, the UV absorption bands are completely bleached upon heating above the spin-transition temperature, making both compounds fully transparent in the HS state within the 250–400 nm spectral region. As evidenced through the thermal transition curves (obtained from the temperature variation of the optical absorbance of the films), these two compounds exhibit very dissimilar SCO behaviors, and thus constitute two different, archetypal examples of thermal spin transition. Indeed, while the thin films of **1** display a very gradual spin conversion, taking place from room temperature to *ca.* 220 °C, the thin films of **2** comparatively exhibit an abrupt transition centered around 64 °C, spanning over a temperature range of only *ca.* 12 °C.

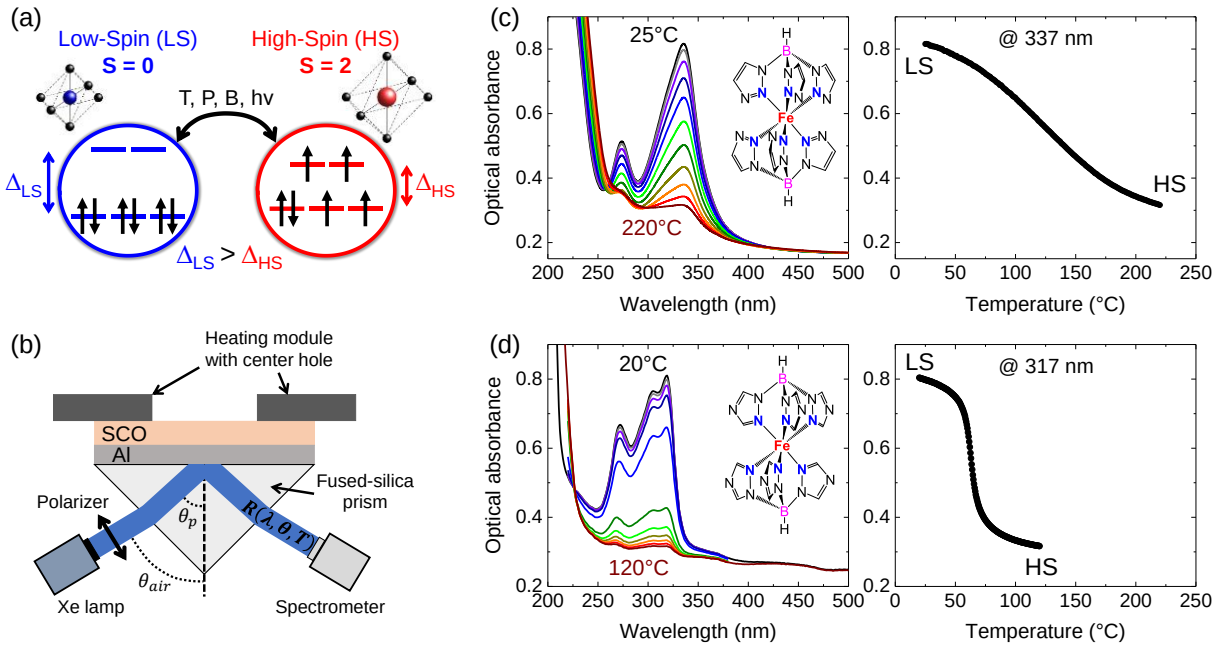

Figure 1. Experimental setup and optical properties of the SCO films. (a) Schematic representation of the 3d electron configurations for an Fe^{2+} SCO complex in its low-spin (LS, $S = 0$) and high-spin (HS, $S = 2$) state. (b) Scheme of the fabricated SCO-based resonant structures, formed by a Al/SCO bilayer deposited on a coupling prism, and excited using the Kretschmann method. (c, d) (left panels) Optical absorbance spectra of (c) a 153-nm-thick film of the complex [Fe(HB(1,2,3-triazol-1-yl)$_3$)$_2$] **1** and (d) a 138-nm-thick film of the complex [Fe(HB(1,2,4-triazol-1-yl)$_3$)$_2$] **2**, acquired at selected temperatures. The films were deposited on fused-silica substrates. The insets show the molecular structure of the two complexes. (c, d) (right panels) Thermal spin-transition curves of the two films extracted from the temperature variation of the optical absorbance at the peak wavelength (λ = 337 and 317 nm for **1** and **2**, respectively).

The fabricated SCO-based optical resonators were investigated by spectroscopic reflectometry measurements performed in the Kretschmann geometry, in the 200–1000 nm spectral domain and within an angular range of θ_{air} = 42–80° in air, which corresponds to incident angles on the Al surface in the range $\theta_p \approx$ 43–68° (taking into account the refraction of the light beam at the air/prism interfaces, see Figure 1b). To obtain absolute values of reflectance, spectra were recorded for both p- and s-polarized incoming light, allowing us to plot the ratio R_p/R_s. The fabricated resonators [prism / Al (16 nm) / SCO (~150 nm)] display different s-polarized and p-polarized resonant optical modes, whose typical dispersion curves (calculated by transfer-matrix methods[40]), are shown, by way of an example, in Figure S1 in the specific case of a non-absorbing dielectric layer. As a comparison, Figure 2a displays the dispersion of resonator **1**, measured by acquiring angle-dependent R_p/R_s spectra, at selected temperatures (between 25 and 220 °C) controlled by bringing the sample in close contact with a heating stage (see Figure 1b). (As an example, the corresponding reflectivity spectra at 25 °C are shown in Figure S2a at selected angles of incidence.) The absorption maxima of the SCO complex in the LS state at λ_{1A} = 337 nm (E_{1A} = 3.68 eV) and λ_{1B} = 274 nm (E_{1B} = 4.52 eV) are depicted in Figure 2 by horizontal white dashed lines. At room temperature, we clearly observe that the dispersion curve of the s-polarized mode (yellow band) is split into three branches at wavelengths λ_{1A} and λ_{1B}, corresponding to the main absorption bands of the SCO complex. As for the p-polarized mode (blue band), the spectra show, within the angular domain probed experimentally, two split peaks around λ_{1A}. Such splitting features in the dispersion are the typical signature of a light-matter hybridization between the molecules and the optical modes, indicating the formation of hybrid light-exciton polaritonic states. As an example, for the p-polarized mode, the maximum splitting is achieved for an incident angle of 76° (indicated by the white double arrow in Figure 2a), where two well-separated, symmetrical peaks are observed with an energy difference of ΔE = 864 meV (see also Figure S2a). This splitting energy is found to be larger than the spectral linewidth of the photon modes ($\Gamma_c \approx$ 300 meV, Q-factor ~12–16) and of the molecular absorption band ($\Gamma_{1A} \approx$ 420 meV), indicating the emergence of a strong-coupling regime.[41,42] Upon heating the sample above the spin-transition temperature, as the molecules are converted into the optically inactive HS state, a progressive decrease of the splitting energies is observed, until the dispersion curves (for both p- and s-polarized modes) virtually show only a single branch, as expected for a non-absorbing dielectric layer. As a result, at 220 °C, unsplit resonances are observed with Q factors of ~16 and ~12 (values taken at 4.2 eV), for the s- and p-polarized modes, respectively.

To model the reflectivity spectra and the angular dispersion of resonator **1**, we used a conventional transfer-matrix method[40] based on Fresnel equations; the resonator being modelled as a multilayer structure composed of optically isotropic and homogeneous layers. The complex refractive index of compound **1** was obtained, for each temperature, by fitting the measured absorbance spectra, shown in Figure 1c, using a Drude-Lorentz oscillator model, where the two main absorption bands were described by Lorentz oscillators (at resonance energies E_{1A} and E_{1B}) displaying temperature-dependent oscillator strengths and damping factors. As shown in Figure 2b, an overall good agreement is obtained

between the experimental and calculated dispersion curves, considering thicknesses of 16 and 160 nm for the aluminum and SCO layers, respectively, which fits well with the nominal experimental values. The anticrossing behavior is well reproduced with maximum energy splitting of *ca.* 800 meV (at constant incident angle) at room temperature, while a progressive vanishing of the splitting is then obtained with increasing temperature, as observed experimentally.

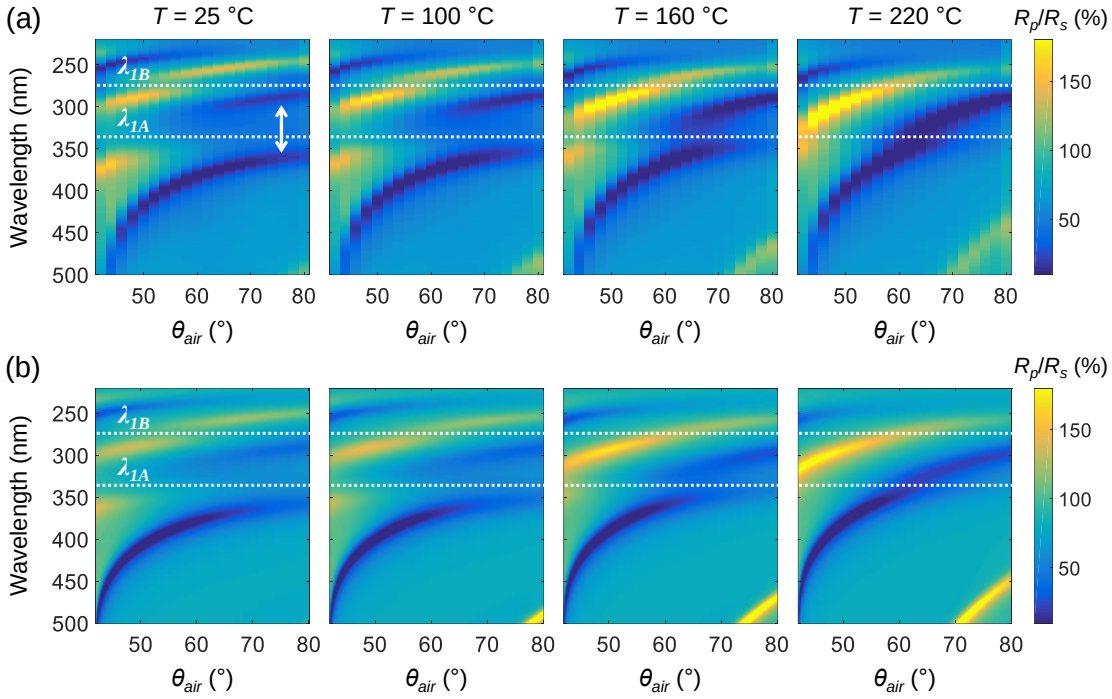

Figure 2. Dispersion of resonator 1 at various temperatures. (a) Experimental dispersion curves of resonator **1** at four different temperatures, obtained by acquiring angle-dependent R_p/R_s spectra within the angular range θ_{air} = 42–80°. (b) Simulated dispersion of the resonator (at the same temperatures) obtained from transfer-matrix calculations (see details in the main text and Experimental Methods). The absorption maxima of the SCO complex in the LS state at λ_{1A} = 337 nm (E_{1A} = 3.68 eV) and λ_{1B} = 274 nm (E_{1B} = 4.52 eV) are depicted by horizontal white dashed lines. The vertical double arrow indicates, as an example, the polaritonic splitting for the p-polarized mode.

To better follow the effect of the thermally induced spin transition, Figure 3 displays the temperature evolution of the p-polarized mode of resonator **1** at a fixed angle of incidence, θ_{air} = 64°, in both heating and cooling modes (the corresponding R_p/R_s spectra are also shown in Figure S2b at selected temperatures). We clearly observe that the Rabi splitting associated with the p-polarized mode, which is coupled to the molecular excitation 1A at room temperature, gradually decreases with temperature, until the two branches merge into a single peak at *ca.* 200–220 °C. As shown in Figure 3, the process is fully reversible since the initial Rabi splitting is totally recovered upon cooling back down to room temperature.

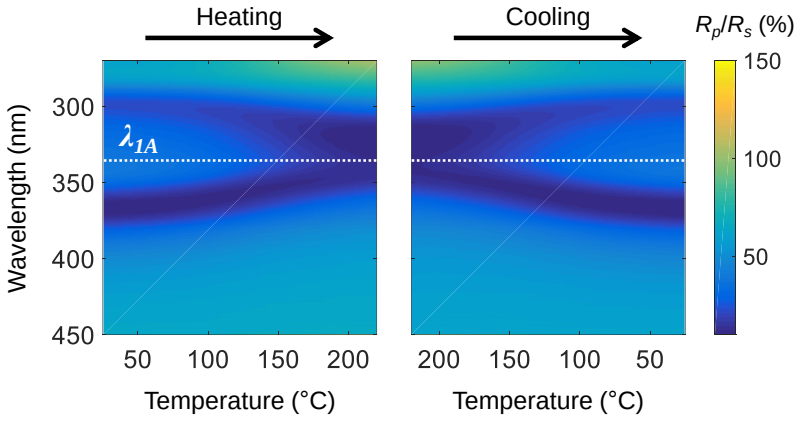

Figure 3. Thermal switching between strong and weak coupling regimes in resonator 1. R_p/R_s spectra acquired at a fixed angle of incidence, θ_{air} = 64°, showing the evolution of the p-polarized mode of resonator **1** as a function of the temperature upon heating and cooling between 25 and 220 °C. The horizontal dashed line at λ_{1A} = 337 nm (E_{1A} = 3.68 eV) indicates the absorption maximum of the SCO complex in the LS state.

To further examine the coupling strength (at constant wave vector) between the optical modes of the resonator and molecular excitons, we have plotted in Figure 4a the extrema energies of the reflectivity spectra, for both s- and p-polarized modes, as a function of the in-plane wave vector k_x. The latter is given by $k_x = (2\pi / \lambda)\, n_p(\lambda) \sin(\theta_p)$ where $n_p(\lambda)$ is the refractive index of the fused-silica prism and θ_p is the incident angle of the light on the Al layer (within the prism). Clear anticrossing behaviors, characteristic of the strong-coupling regime, are observed at energies corresponding to the maximum absorption of LS molecules. In order to evaluate the coupling strengths, we employed a quantum mechanical coupled-oscillator model to fit the experimental dispersion curves (solid lines in Figure 4a), the polariton bands of the coupled system being given by the eigenvalues of the following Hamiltonian:

$$\hat{\mathcal{H}} = \begin{pmatrix} E_c(k_x) & \hbar\Omega_{RA}/2 & \hbar\Omega_{RB}/2 \\ \hbar\Omega_{RA}/2 & E_A & 0 \\ \hbar\Omega_{RB}/2 & 0 & E_B \end{pmatrix} \quad (1)$$

where $E_c(k_x)$ is the dispersion relation of the bare photon mode, E_A and E_B are the dispersionless exciton modes of SCO molecules, and $\hbar\Omega_{RA}$ and $\hbar\Omega_{RB}$ are the corresponding Rabi-splitting energies. At room temperature (25 °C), for the s-polarized mode, the fitting reveals that the resonances occur for k_x = 18.2 and 28.1 µm^{-1} (when the uncoupled photon mode has the same energy as the molecular excitations 1A and 1B), with corresponding Rabi-splitting energies of 546 and 259 meV, respectively. As for the p-polarized mode, the coupling between the optical resonator and molecules at E_{1A} is characterized by a Rabi-splitting energy of 535 meV. These light-matter interaction energy values, which correspond (in the case of the molecular excitation 1A) to 15 % of the bare energy of the uncoupled systems, $\eta = \hbar\Omega_{RA} / E_{1A} \approx 0.15$, signify that our SCO-based resonator is likely into the so-called ultrastrong-coupling (USC) regime.[43,44] The latter is indeed generally considered as established when the normalized coupling factor is $\eta > 0.1$. This USC regime is currently the subject of intense investigations due to the potential emergence of intriguing physical effects and applications, including fast and protected quantum

information processing, nonlinear optics, modified chemical reactivity, or the enhancement of various quantum phenomena.[43] Especially, this regime is particularly interesting since it implies that not only the excited states of the coupled system are disturbed but also the ground state,[45,46] which could possibly have an effect on the thermodynamics of molecules and, therefore, on their switching properties.[22,47,48] This point will be discussed in more detail later in the article. At this stage, it is worth mentioning that the use of relatively low light intensities (below 0.25 mW cm^{-2} in the wavelength range of interest [250–400 nm]) ensures that the current studies are performed within the vacuum ultrastrong-coupling regime, as it was further confirmed by the independence of the measured Rabi-splitting energies with the incident light intensity. Finally, as shown in Figure 4a, a clear diminution of the coupling strength is observed upon heating, and, at 220 °C (almost fully in the HS state), the maximum splitting energy is found to be 172 meV (for the molecular excitation 1A), which indicates that the system lies in the weak-coupling regime.

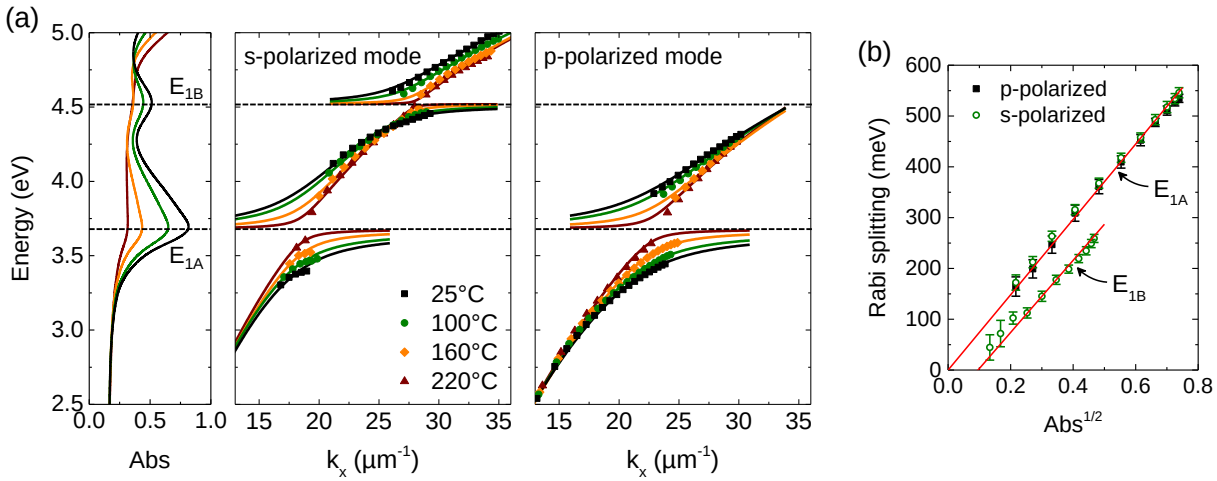

Figure 4. Dispersion (energy vs. in-plane wave vector) curves of resonator 1 and dependence of the Rabi-splitting energies upon SCO film absorbance. (a) Measured dispersion curves of resonator **1**, for both s- and p-polarized modes, at selected temperatures between 25 and 220 °C. The horizontal dashed lines at E_{1A} = 3.68 eV and E_{1B} = 4.52 eV indicate the dispersionless molecular excitation energies. The fits (solid lines) of the dispersion curves of the coupled system are obtained using a three-coupled oscillator model whose Hamiltonian is given by Equation (1). (b) Evolution of the Rabi-splitting energies – extracted from the fitting procedure in (a) – as a function of the square root of the SCO film absorbance. Error bars represent one standard deviation of the fitted Rabi-splitting values.

As depicted in Figure 4b, the Rabi-splitting energy extracted from the fitting procedure at the resonance with the molecular excitation 1A is found to be closely proportional to the square root of the SCO film absorbance, which is an expected feature since the Rabi splitting is known to scale with the square root of the concentration of coupled molecules (here LS molecules) within the optical mode volume.[4] Interestingly, the coupling strength of the optical resonator with the molecular excitation 1A is found to be identical (within the error bars) for both s- and p-polarized modes, meaning that the

electric field amplitude distribution, averaged over the total thickness of the SCO layer, is similar for both s- and p-polarized modes. However, noticeable differences are observed when comparing the coupling strength of the s-polarized optical mode with the two molecular excitations 1A and 1B. Such differences presumably come from a greater mismatch between photon and exciton linewidths in the case of the molecular excitation 1B, which has the effect, as observed experimentally, of reducing the Rabi-splitting energy and deviating the evolution of $\hbar\Omega_R$ with respect to $Abs^{1/2}$ from the linear behavior.[5]

In a similar manner, we have also investigated the spectroscopic characteristics of resonator **2**, which incorporates a 138-nm-thick film of the complex [Fe(HB(1,2,4-triazol-1-yl)$_3$)$_2$]. In the angular range studied, the experimental dispersion curves reveal that only a p-polarized mode of the optical resonator enters into resonance with the molecular excitations. As displayed in Figure 5a (see also the corresponding spectra in Figure S3), at room temperature, this mode is split into three branches at wavelengths $\lambda_{2A} \approx 315$ nm ($E_{2A} \approx 3.93$ eV) and $\lambda_{2B} = 272$ nm ($E_{2B} = 4.55$ eV), corresponding to the two main absorption bands of the complex in the LS state (the effects of the two molecular excitations at 305 and 317 nm are experimentally indistinguishable due to their spectral proximity so that they are considered as a single band). When the sample is heated, a sudden decrease of the splitting energies is observed between 60 and 80 °C, corresponding to the switching of complex **2** from the LS to the HS state. As displayed in Figure S4, a good agreement is found between the experimental and simulated dispersion curves obtained by transfer-matrix calculations, for the different temperatures studied. The effect of the spin transition is shown in more detail in Figure 5b, where the temperature evolution of the resonant modes is recorded at a fixed angle of incidence, $\theta_{air} = 74°$, upon heating and cooling. On one hand, an abrupt decrease of the Rabi splitting is evidenced for the (coupled) p-polarized mode around $T_{SCO} = 64$ °C, above which temperature only a single branch is observed. On the other hand, the uncoupled s-polarized mode (at $\lambda \approx 440$ nm, i.e. far from any molecular absorption) simultaneously exhibits a marked 30-nm blue shift due to the SCO phenomenon. This blue shift is attributed to the substantial decrease of the refractive index of the SCO material (by *ca.* 4 % in the visible domain) when switching from the LS to the HS state[31] (see Figure S5). Thus, in addition to the coupling/uncoupling process with molecular excitons, the resonant optical modes are also impacted by the refractive index change of the SCO layer upon the spin transition, providing a dual mode of tuning based either on the absorption change or on the refractive index modulation.

As depicted in Figure 5b, these SCO-induced phenomena are fully reversible when coming back to room temperature. For the sake of completeness, two additional heating/cooling cycles were measured (see Figure S6), which further demonstrates the reproducible character of the switching between coupled and uncoupled states induced by thermal cycling. From this point of view, it is worth noting that the use of vacuum-deposited molecular films is advantageous because these films are known to exhibit high stability and robustness of the spin-transition properties as well as an exceptionally high switching endurance (>10^7 thermal switching events in films of **2**)[49] upon repeated cycling.

The dispersion (energy vs. in-plane wave vector) curves of resonator **2**, shown in Figure 5c, reveal Rabi-splitting energies up to 548 and 192 meV at room temperature (full LS state), at the resonance with the two main molecular absorption bands 2A and 2B, respectively. In this case, this maximum Rabi-splitting energy corresponds to 14 % of the molecular excitation energy, which indicates, as for resonator **1**, an ultrastrong coupling regime. Above 100 °C, no splitting is detectable as the SCO film is fully in the non-absorbing HS state.

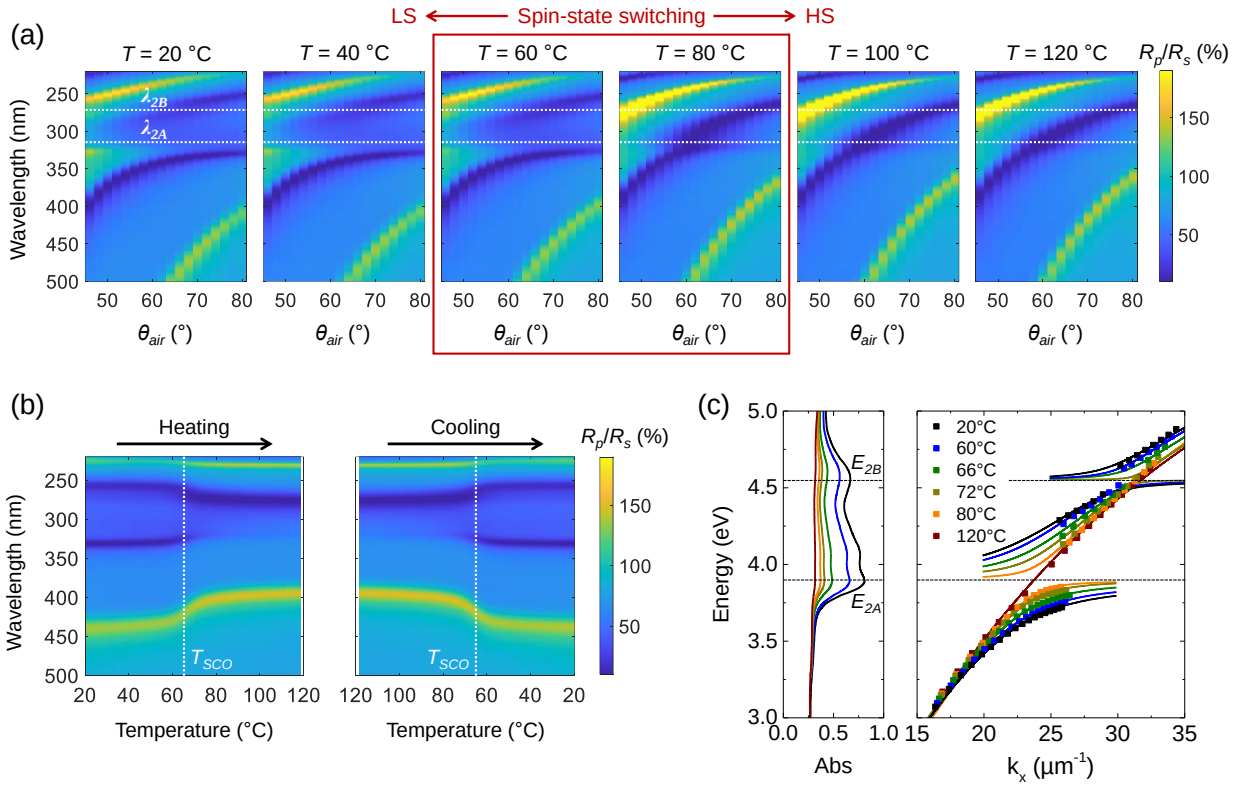

Figure 5. Spectroscopic characteristics of resonator 2. (a) Dispersion of resonator **2** at six different temperatures, obtained by acquiring angle-dependent R_p/R_s spectra within the range θ_{air} = 46–80°. The two main absorption maxima of the SCO complex in the LS state at λ_{2A} = 315 nm (E_{2A} = 3.93 eV) and λ_{2B} = 272 nm (E_{2B} = 4.55 eV) are depicted by horizontal white dashed lines. (b) R_p/R_s spectra measured at a fixed angle of incidence, θ_{air} = 74°, showing the evolution of the p- and s-polarized modes as a function of the temperature upon heating and cooling between 20 and 120 °C. The white dashed lines indicate the spin-transition temperature T_{SCO} = 64 °C. (c) Dispersion curves (energy vs. in-plane wave vector) of resonator **2** (p-polarized mode) at selected temperatures between 20 and 120 °C. The horizontal dashed lines at 3.93 and 4.55 eV indicate the dispersionless molecular excitation energies. The fits (solid lines) are obtained using a three-coupled oscillator model whose Hamiltonian is given by Equation (1).

Importantly, the abrupt and well-reproducible character of the spin transition in films of **2** also offers the possibility of carefully analyzing a potential effect of the strong-coupling regime on the thermally induced spin-transition properties. Interestingly, the spectral shift of the s-polarized resonance, observed in response to the SCO-induced change of the refractive index, allows the evolution

of the thermal spin transition in the coupled film (inside the resonator) to be accurately investigated. By comparing this thermal shift with the variation of the optical absorbance of a bare SCO film (outside of the resonator) under the same heating/cooling rates (1 °C min^{-1}), we show that the spin-crossover properties (i.e., abruptness and temperature of the spin transition) of the film coupled to the optical resonator remain essentially unaltered (see Figure S7). Put differently, beyond experimental uncertainty, it appears that neither the energy gap between the HS and LS states, nor the cooperativity of the spin transition is affected by the (ultra)strong light-matter coupling. These results are in line with those obtained using other photoswitchable molecules, like spiropyrans[13] and norbornadienes[50], for which a significant change in the kinetics of the photoisomerisation reaction was evidenced under strong coupling, but no effect was reported on the rate of the thermally induced back conversion process, indicating that the ground state is unaffected by the formation of polaritonic states.

In the past decade, the effect of strong coupling on the ground-state properties and reactivity of molecules has attracted much attention,[10,14,22,47,51,52] but the origin of the exciting experimental findings remains largely open to discussion. The generally accepted picture is that for a macroscopic system with $N >> 1$ dipoles, the resonant-coupling-induced change to the free energy becomes negligible[53–57] and thus other, still debated, mechanisms must prevail. Notably, theoretical calculations indicated that strong coupling between the dipole moment (μ) of SCO molecules and the confined EM field in plasmonic nanocavities could give rise to a substantial shift of the spin-state equilibrium temperature – provided that μ is aligned with the polarization of the cavity mode and displays a sizeable change upon the spin transition.[48] These conditions are, effectively, not met in our experiments due to the high symmetry of the studied molecules, which results in extremely small permanent dipole moments (*ca.* 0.001 and 0.0002 Debye in the HS and LS states, respectively, for compound **2**).[58] Further work should therefore focus on using molecules exhibiting large dipole moment differences between the two spin states and photonic resonators with more tightly confined EM fields.

As a summary, Figure 6 displays the temperature evolution of the Rabi-splitting energies measured in the two studied optical resonators, demonstrating the possibility of a thermal tunability of the light-molecule coupling strength, between a strong and weak coupling regime. We show that this regime change follows the characteristics of the thermal spin transition. Interestingly, the two resonators studied here represent two antagonist cases: while resonator **1** exhibits a very gradual tuning of the hybridization strength on a wide temperature range (then allowing a tight external control of the coupling strength), resonator **2** shows a relatively abrupt ON/OFF switching of the coupling regime. As discussed previously, it is worth mentioning that in both cases the switching between the ultrastrong and weak coupling regimes can be achieved reversibly and in a fully reproducible manner.

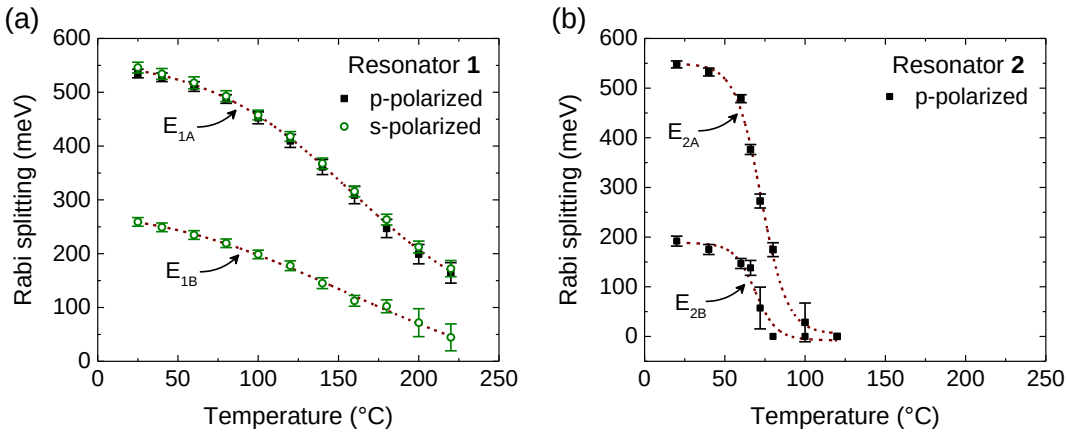

Figure 6. Tunability of the light-matter coupling strength with temperature in the two resonators studied. Temperature evolution of the Rabi-splitting energies measured in (a) resonator **1** and (b) resonator **2**, incorporating a SCO thin film of complex [Fe(HB(1,2,3-triazol-1-yl)$_3$)$_2$] **1** and [Fe(HB(1,2,4-triazol-1-yl)$_3$)$_2$] **2**, respectively. Error bars represent one standard deviation of the fitted Rabi-splitting values. The dashed lines are guides for the eye.

In conclusion, we have demonstrated a switchable ultrastrong light-matter coupling between optical modes of metal/dielectric bilayer resonators and spin-crossover molecules. In their LS form, the intense absorption bands of SCO molecules in the UV spectral domain can be coupled to resonant photon modes resulting in Rabi-splitting energies up to 550 meV, i.e. 15 % of the molecular excitation energy. By converting thermally the molecules into their non-absorbing HS state, we demonstrate the possibility of fine-tuning the light-matter hybridization strength, ultimately allowing a reversible and reproducible switching between ultrastrong and weak coupling regimes in a single photonic system. Interestingly, using vacuum-deposited thin films of two SCO compounds with different spin-transition properties, a gradual and abrupt switching of the coupling regime could be achieved with temperature.

Through this work, we show that SCO compounds constitute a class of stimuli-responsive molecular materials of great interest in the field of switchable polaritonic chemistry as well as in the domain of active photonics. In this perspective, an appealing feature of SCO compounds is the possibility to use light irradiation to address the molecular spin state. As the photoswitching process typically occurs on the sub-picosecond timescale,[39] this suggests interesting prospects for ultrafast all-optical modulation of the strong light-matter coupling in micro-nano-cavities, governed by short laser excitations. In addition, the vast library of well-characterized SCO materials, exhibiting a variety of spin-transition properties (gradual, abrupt, with or without hysteretic behaviors), provides an excellent playground for the investigation and the design of appealing switchable polaritonic systems.

On the other way around, this study also opens up the possibility to explore the physical and chemical properties of switchable SCO molecules under strong coupling. In particular, an interesting aspect would be to probe the effect of this coupling on the photophysical properties of molecules (by ultrafast optical spectroscopic methods), the present results paving the way, as an example, for detailed

studies on the dynamics of the polaritonic states as a function of the coupling strength in a single optical cavity. Another appealing perspective is to investigate the possible effects of the light-matter hybridization on the molecular ground state and, therefore, on the LS/HS phase equilibrium of coupled molecules. Within our experimental conditions, we have not observed any noticeable effect of the USC regime on the SCO behavior. Yet, the extreme robustness and reproducibility of the SCO phenomenon in our preferentially-oriented, thin films (>10 million thermal switching events with <1 °C drift in films of **2**)[49] provides a very appealing scope to analyze even minute effects of the USC regime on the ground state of the system. In addition, within this family of scorpionate ligand complexes, several other SCO compounds show interesting properties such as photoswitching effect, hysteretic behavior and/or a significant change in dipole moment upon SCO, which could be appealing assets in the context of molecular polaritonics. This work is currently ongoing in our laboratories.

Experimental Methods

Spin-crossover sample synthesis and optical resonator fabrication. The bulk powder of compounds **1** and **2** was synthesized as previously described in refs. 35 and 36, respectively. The Al/SCO bilayer resonators were fabricated by first depositing a 16-nm-thick film of aluminum on the hypotenuse face (of size 1 × 1.41 cm^2) of fused-silica right-angle prisms, then coated with a SCO film of either compound **1** (153 nm thick) or compound **2** (138 nm thick). Both Al and SCO films were grown by thermal evaporation. The bulk powder of SCO complexes was heated at *ca.* 240 °C in a quartz crucible at a base pressure of 2×10^{-7} mbar. Film thicknesses were monitored in situ using a quartz crystal microbalance and ex situ by spectral reflectance measurements (Filmetrics, F20). The as-deposited films of **1** are dense and crystalline with a preferred [011] orientation of the monoclinic crystal lattice normal to the substrate surface.[38] The as-deposited films of **2** were recrystallized by a solvent-vapor annealing treatment, resulting in oriented, nanocrystalline thin films.[37]

Spectroscopic characterization. The fabricated SCO-based resonators were investigated by spectroscopic reflectometry measurements, in the 200–1000 nm spectral domain and within an angular range of θ_{air} = 42–80° in air. The samples were illuminated by a pulsed xenon lamp (Avantes, AvaLight-XE-HP) and the incoming beam was collimated and spatially limited to a diameter of 5 mm with an aperture. A Glan-Laser α-BBO polarizer is inserted in the path of the light source to obtain either s- or p-polarized light and the reflected light was collected by a fiber-coupled spectrometer (Avantes, AvaSpec-ULS2048CL-EVO). The temperature of the sample was controlled in situ by bringing the SCO layer of the resonator in close contact with a heating stage (Linkam Scientific, PE120 or FTIRSP600), which presents a center hole in order to keep air as the last dielectric layer in the probe region of the structure (see the experimental setup in Figure 1b).

Transfer-matrix simulations. The reflectivity spectra and angular dispersion of resonators **1** and **2** were simulated using conventional transfer-matrix calculations.[40] The fabricated optical resonators were modelled as a multilayer structure, which consists of semi-infinite space of fused silica, a layer of

aluminum, a dielectric (SCO material) layer and a semi-infinite space of air. The actual angles θ_p at which the incoming beam hits the Al surface within the prism were obtained from the experimental incident angles in air, θ_{air}, by taking into account the refraction of the light beam at the air-prism interface. Calculations were performed including the known optical properties of fused silica[59] and aluminum,[60] while the frequency-dependent refractive index of the SCO compounds was obtained from the measured UV-vis absorbance spectra (and from previously reported temperature-dependent ellipsometric data[31] in the case of compound **2**) using a Drude-Lorentz oscillator model.

ASSOCIATED CONTENT

Supporting Information

Typical dispersion curves of the fabricated optical resonators, calculated by transfer-matrix simulations, in the case of a non-dispersive and non-absorbing dielectric medium. Additional spectroscopic characteristics of resonators **1** and **2**: reflectivity R_p/R_s spectra for different angles of incidence and for various selected temperatures upon heating and cooling. Comparison between experimental and simulated dispersion curves of resonator **2** at various temperatures. Temperature dependence of the refractive index n of a thin film of **2** at selected wavelengths. R_p/R_s spectra of resonator **2** for two additional heating/cooling cycles. Comparison of thermal spin-transition curves of a bare SCO film of **2** and of the coupled film in resonator **2**.

AUTHOR INFORMATION

Corresponding Authors

Karl Ridier – Laboratoire de Chimie de Coordination, CNRS UPR 8241, Université de Toulouse, F-31077 Toulouse, France ; Email: karl.ridier@lcc-toulouse.fr

Azzedine Bousseksou – Laboratoire de Chimie de Coordination, CNRS UPR 8241, Université de Toulouse, F-31077 Toulouse, France ; Email: azzedine.bousseksou@lcc-toulouse.fr

Authors

Lijun Zhang – Laboratoire de Chimie de Coordination, CNRS UPR 8241, Université de Toulouse, F-31077 Toulouse, France

Oleksandr Ye. Horniichuk – Laboratoire de Chimie de Coordination, CNRS UPR 8241, Université de Toulouse, F-31077 Toulouse, France

Stéphane Calvez – Laboratoire d'Analyse et d'Architecture des Systèmes, CNRS UPR 8001, Université de Toulouse, F-31400 Toulouse, France

Lionel Salmon – Laboratoire de Chimie de Coordination, CNRS UPR 8241, Université de Toulouse, F-31077 Toulouse, France

Gábor Molnár – Laboratoire de Chimie de Coordination, CNRS UPR 8241, Université de Toulouse, F-31077 Toulouse, France

Notes

The authors declare no competing financial interest.

ACKNOWLEDGMENTS

This work received financial support from the Agence Nationale de la Recherche (project SCOPOL, ANR-22-CE09-0019), the University of Toulouse III (project AO Tremplin "MaCaPeSuMO") and the Centre National de la Recherche Scientifique (project MITI "CMTS-SLM"). Part of the work was conducted at the LAAS-CNRS micro and nanotechnologies platform, which is a member of the French RENATECH network of cleanroom facilities. L.Z. thanks China Scholarship Council for a PhD grant. O.Y.H. acknowledges the French Embassy in Ukraine and Campus France for a BGF scholarship.

REFERENCES

(1) Ebbesen, T. W. Hybrid Light–Matter States in a Molecular and Material Science Perspective. *Acc. Chem. Res.* **2016**, *49*, 2403–2412.

(2) Ribeiro, R. F.; Martínez-Martínez, L. A.; Du, M.; Campos-Gonzalez-Angulo, J.; Yuen-Zhou, J. Polariton Chemistry: Controlling Molecular Dynamics with Optical Cavities. *Chem. Sci.* **2018**, *9*, 6325–6339.

(3) Dovzhenko, D. S.; Ryabchuk, S. V.; Rakovich, Y. P.; Nabiev, I. R. Light–Matter Interaction in the Strong Coupling Regime: Configurations, Conditions, and Applications. *Nanoscale* **2018**, *10*, 3589–3605.

(4) Hertzog, M.; Wang, M.; Mony, J.; Börjesson, K. Strong Light–Matter Interactions: A New Direction within Chemistry. *Chem. Soc. Rev.* **2019**, *48*, 937–961.

(5) Herrera, F.; Owrutsky, J. Molecular Polaritons for Controlling Chemistry with Quantum Optics. *J. Chem. Phys.* **2020**, *152*, 100902.

(6) Garcia-Vidal, F. J.; Ciuti, C.; Ebbesen, T. W. Manipulating Matter by Strong Coupling to Vacuum Fields. *Science* **2021**, *373*, 178.

(7) Lidzey, D. G.; Bradley, D. D. C.; Skolnick, M. S.; Virgili, T.; Walker, S.; Whittaker, D. M. Strong Exciton–Photon Coupling in an Organic Semiconductor Microcavity. *Nature* **1998**, *395*, 53–55.

(8) Schwartz, T.; Hutchison, J. A.; Genet, C.; Ebbesen, T. W. Reversible Switching of Ultrastrong Light-Molecule Coupling. *Phys. Rev. Lett.* **2011**, *106*, 196405.

(9) Shalabney, A.; George, J.; Hutchison, J.; Pupillo, G.; Genet, C.; Ebbesen, T. W. Coherent Coupling of Molecular Resonators with a Microcavity Mode. *Nat. Commun.* **2015**, *6*, 5981.

(10) Thomas, A.; George, J.; Shalabney, A.; Dryzhakov, M.; Varma, S. J.; Moran, J.; Chervy, T.; Zhong, X.; Devaux, E.; Genet, C.; Hutchison, J. A.; Ebbesen, T. W. Ground-State Chemical Reactivity under Vibrational Coupling to the Vacuum Electromagnetic Field. *Angew. Chem. Int. Ed.* **2016**, *55*, 11462–11466.

(11) Hobson, P. A.; Barnes, W. L.; Lidzey, D. G.; Gehring, G. A.; Whittaker, D. M.; Skolnick, M. S.; Walker, S. Strong Exciton–Photon Coupling in a Low-Q All-Metal Mirror Microcavity. *Appl. Phys. Lett.* **2002**, *81*, 3519–3521.

(12) Feist, J.; Galego, J.; Garcia-Vidal, F. J. Polaritonic Chemistry with Organic Molecules. *ACS Photonics* **2018**, *5*, 205–216.

(13) Hutchison, J. A.; Schwartz, T.; Genet, C.; Devaux, E.; Ebbesen, T. W. Modifying Chemical Landscapes by Coupling to Vacuum Fields. *Angew. Chem. Int. Ed.* **2012**, *51*, 1592–1596.

(14) Thomas, A.; Jayachandran, A.; Lethuillier-Karl, L.; Vergauwe, R. M. A.; Nagarajan, K.; Devaux, E.; Genet, C.; Moran, J.; Ebbesen, T. W. Ground State Chemistry under Vibrational Strong Coupling: Dependence of Thermodynamic Parameters on the Rabi Splitting Energy. *Nanophotonics* **2020**, *9*, 249–255.
(15) Lather, J.; Bhatt, P.; Thomas, A.; Ebbesen, T. W.; George, J. Cavity Catalysis by Cooperative Vibrational Strong Coupling of Reactant and Solvent Molecules. *Angew. Chem. Int. Ed.* **2019**, *58*, 10635–10638.
(16) Orgiu, E.; George, J.; Hutchison, J. A.; Devaux, E.; Dayen, J. F.; Doudin, B.; Stellacci, F.; Genet, C.; Schachenmayer, J.; Genes, C.; Pupillo, G.; Samorì, P.; Ebbesen, T. W. Conductivity in Organic Semiconductors Hybridized with the Vacuum Field. *Nat. Mater.* **2015**, *14*, 1123–1129.
(17) Hutchison, J. A.; Liscio, A.; Schwartz, T.; Canaguier-Durand, A.; Genet, C.; Palermo, V.; Samorì, P.; Ebbesen, T. W. Tuning the Work-Function Via Strong Coupling. *Adv. Mater.* **2013**, *25*, 2481–2485.
(18) Baudrion, A.-L.; Perron, A.; Veltri, A.; Bouhelier, A.; Adam, P.-M.; Bachelot, R. Reversible Strong Coupling in Silver Nanoparticle Arrays Using Photochromic Molecules. *Nano Lett.* **2013**, *13*, 282–286.
(19) Lin, L.; Wang, M.; Wei, X.; Peng, X.; Xie, C.; Zheng, Y. Photoswitchable Rabi Splitting in Hybrid Plasmon–Waveguide Modes. *Nano Lett.* **2016**, *16*, 7655–7663.
(20) Asamoah, B. O.; Mohamed, S.; Datta, S.; Karvinen, P.; Rekola, H.; Priimagi, A.; Hakala, T. K. Optically Induced Crossover from Weak to Strong Coupling Regime between Surface Plasmon Polaritons and Photochromic Molecules. *Opt. Express* **2020**, *28*, 26509–26518.
(21) Thomas, P. A.; Menghrajani, K. S.; Barnes, W. L. All-Optical Control of Phase Singularities Using Strong Light-Matter Coupling. *Nat. Commun.* **2022**, *13*, 1809.
(22) Wang, S.; Mika, A.; Hutchison, J. A.; Genet, C.; Jouaiti, A.; Hosseini, M. W.; Ebbesen, T. W. Phase Transition of a Perovskite Strongly Coupled to the Vacuum Field. *Nanoscale* **2014**, *6*, 7243–7248.
(23) Ashida, Y.; İmamoğlu, A.; Faist, J.; Jaksch, D.; Cavalleri, A.; Demler, E. Quantum Electrodynamic Control of Matter: Cavity-Enhanced Ferroelectric Phase Transition. *Phys. Rev. X* **2020**, *10*, 041027.
(24) Chang, Y.-W.; Yao, J.; Zhu, X.-F.; Wei, Q.; Wu, D.-J. Alternating Coupling Regimes in a Plasmon–Molecule Hybrid Structure through a Phase-Change Material. *J. Phys. Chem. C* **2020**, *124*, 22671–22676.
(25) Gütlich, P.; Hauser, A.; Spiering, H. Thermal and Optical Switching of Iron(II) Complexes. *Angew. Chem. Int. Ed.* **1994**, *33*, 2024–2054.
(26) Gütlich, P.; Goodwin, H. A. *Spin Crossover in Transition Metal Compounds I-III*. (Springer-Verlag, Berlin, Heidelberg, 2004).
(27) Bousseksou, A.; Molnár, G.; Salmon, L.; Nicolazzi, W. Molecular Spin Crossover Phenomenon: Recent Achievements and Prospects. *Chem. Soc. Rev.* **2011**, *40*, 3313–3335.
(28) Kahn, O.; Kröber, J.; Jay, C. Spin Transition Molecular Materials for Displays and Data Recording. *Adv. Mater.* **1992**, *4*, 718–728.
(29) Félix, G.; Abdul-Kader, K.; Mahfoud, T.; Gural'skiy, I. A.; Nicolazzi, W.; Salmon, L.; Molnár, G.; Bousseksou, A. Surface Plasmons Reveal Spin Crossover in Nanometric Layers. *J. Am. Chem. Soc.* **2011**, *133*, 15342–15345.
(30) Iazzolino, A.; Galle, G.; Degert, J.; Létard, J. F.; Freysz, E. Impact of the Spin State Switching on the Dielectric Constant of Iron (II) Spin Crossover Nanoparticles. *Chem. Phys. Lett.* **2015**, *641*, 14–19.

(31) Zhang, Y.; Ridier, K.; Shalabaeva, V.; Séguy, I.; Pelloquin, S.; Camon, H.; Calvez, S.; Routaboul, L.; Salmon, L.; Molnár, G.; Bousseksou, A. A Molecular Spin-Crossover Film Allows for Wavelength Tuning of the Resonance of a Fabry–Perot Cavity. *J. Mater. Chem. C* **2020**, *8*, 8007–8011.
(32) Abdul-Kader, K.; Lopes, M.; Bartual-Murgui, C.; Kraieva, O.; Hernández, E. M.; Salmon, L.; Nicolazzi, W.; Carcenac, F.; Thibault, C.; Molnár, G.; Bousseksou, A. Synergistic Switching of Plasmonic Resonances and Molecular Spin States. *Nanoscale* **2013**, *5*, 5288–5293.
(33) Akou, A.; Bartual-Murgui, C.; Abdul-Kader, K.; Lopes, M.; Molnár, G.; Thibault, C.; Vieu, C.; Salmon, L.; Bousseksou, A. Photonic Gratings of the Metal–Organic Framework {Fe(bpac)[Pt(CN)$_4$]} with Synergetic Spin Transition and Host–Guest Properties. *Dalton Trans.* **2013**, *42*, 16021–16028.
(34) Palluel, M.; Tran, N. M.; Daro, N.; Buffière, S.; Mornet, S.; Freysz, E.; Chastanet, G. The Interplay between Surface Plasmon Resonance and Switching Properties in Gold@Spin Crossover Nanocomposites. *Adv. Funct. Mater.* **2020**, *30*, 2000447.
(35) Horniichuk, O. Y.; Ridier, K.; Molnár, G.; Kotsyubynsky, V. O.; Shova, S.; Amirkhanov, V. M.; Gural'skiy, I. A.; Salmon, L.; Bousseksou, A. Solvatomorphism, Polymorphism and Spin Crossover in bis[hydrotris(1,2,3-triazol-1-yl)borate]iron(II). *New J. Chem.* **2022**, *46*, 11734–11740.
(36) Rat, S.; Ridier, K.; Vendier, L.; Molnár, G.; Salmon, L.; Bousseksou, A. Solvatomorphism and Structural-Spin Crossover Property Relationship in bis[hydrotris(1,2,4-triazol-1-yl)borate]iron(II). *CrystEngComm* **2017**, *19*, 3271–3280.
(37) Shalabaeva, V.; Rat, S.; Manrique-Juarez, M. D.; Bas, A.-C.; Vendier, L.; Salmon, L.; Molnár, G.; Bousseksou, A. Vacuum Deposition of High-Quality Thin Films Displaying Spin Transition near Room Temperature. *J. Mater. Chem. C* **2017**, *5*, 4419–4425.
(38) Horniichuk, O. Ye.; Ridier, K.; Zhang, L.; Zhang, Y.; Molnár, G.; Salmon, L.; Bousseksou, A. High-Sensitivity Microthermometry Method Based on Vacuum-Deposited Thin Films Exhibiting Gradual Spin Crossover above Room Temperature. *ACS Appl. Mater. Interfaces* **2022**, *14*, 52140–52148.
(39) Ridier, K.; Bas, A.-C.; Shalabaeva, V.; Nicolazzi, W.; Salmon, L.; Molnár, G.; Bousseksou, A.; Lorenc, M.; Bertoni, R.; Collet, E.; Cailleau, H. Finite Size Effects on the Switching Dynamics of Spin-Crossover Thin Films Photoexcited by a Femtosecond Laser Pulse. *Adv. Mater.* **2019**, *31*, 1901361.
(40) Katsidis, C. C.; Siapkas, D. I. General Transfer-Matrix Method for Optical Multilayer Systems with Coherent, Partially Coherent, and Incoherent Interference. *Appl. Opt.* **2002**, *41*, 3978–3987.
(41) Törmä, P.; Barnes, W. L. Strong Coupling between Surface Plasmon Polaritons and Emitters: A Review. *Rep. Prog. Phys.* **2015**, *78*, 013901.
(42) Thomas, P. A.; Tan, W. J.; Fernandez, H. A.; Barnes, W. L. A New Signature for Strong Light–Matter Coupling Using Spectroscopic Ellipsometry. *Nano Lett.* **2020**, *20*, 6412–6419.
(43) Frisk Kockum, A.; Miranowicz, A.; De Liberato, S.; Savasta, S.; Nori, F. Ultrastrong Coupling between Light and Matter. *Nat. Rev. Phys.* **2019**, *1*, 19–40.
(44) Forn-Díaz, P.; Lamata, L.; Rico, E.; Kono, J.; Solano, E. Ultrastrong Coupling Regimes of Light-Matter Interaction. *Rev. Mod. Phys.* **2019**, *91*, 025005.
(45) Ciuti, C.; Bastard, G.; Carusotto, I. Quantum Vacuum Properties of the Intersubband Cavity Polariton Field. *Phys. Rev. B* **2005**, *72*, 115303.
(46) Forn-Díaz, P.; Lisenfeld, J.; Marcos, D.; García-Ripoll, J. J.; Solano, E.; Harmans, C. J. P. M.; Mooij, J. E. Observation of the Bloch-Siegert Shift in a Qubit-Oscillator System in the Ultrastrong Coupling Regime. *Phys. Rev. Lett.* **2010**, *105*, 237001.

(47) Canaguier-Durand, A.; Devaux, E.; George, J.; Pang, Y.; Hutchison, J. A.; Schwartz, T.; Genet, C.; Wilhelms, N.; Lehn, J.-M.; Ebbesen, T. W. Thermodynamics of Molecules Strongly Coupled to the Vacuum Field. *Angew. Chem. Int. Ed.* **2013**, *52*, 10533–10536.
(48) Climent, C.; Galego, J.; Garcia-Vidal, F. J.; Feist, J. Plasmonic Nanocavities Enable Self-Induced Electrostatic Catalysis. *Angew. Chem. Int. Ed.* **2019**, *58*, 8698–8702.
(49) Ridier, K.; Bas, A.-C.; Zhang, Y.; Routaboul, L.; Salmon, L.; Molnár, G.; Bergaud, C.; Bousseksou, A. Unprecedented Switching Endurance Affords for High-Resolution Surface Temperature Mapping Using a Spin-Crossover Film. *Nat. Commun.* **2020**, *11*, 3611.
(50) Mony, J.; Climent, C.; Petersen, A. U.; Moth-Poulsen, K.; Feist, J.; Börjesson, K. Photoisomerization Efficiency of a Solar Thermal Fuel in the Strong Coupling Regime. *Adv. Funct. Mater.* **2021**, *31*, 2010737.
(51) Thomas, A.; Lethuillier-Karl, L.; Nagarajan, K.; Vergauwe, R. M. A.; George, J.; Chervy, T.; Shalabney, A.; Devaux, E.; Genet, C.; Moran, J.; Ebbesen, T. W. Tilting a Ground-State Reactivity Landscape by Vibrational Strong Coupling. *Science* **2019**, *363*, 615–619.
(52) Simpkins, B. S.; Dunkelberger, A. D.; Owrutsky, J. C. Mode-Specific Chemistry through Vibrational Strong Coupling (or A Wish Come True). *J. Phys. Chem. C* **2021**, *125*, 19081–19087.
(53) Ćwik, J. A.; Kirton, P.; De Liberato, S.; Keeling, J. Excitonic Spectral Features in Strongly Coupled Organic Polaritons. *Phys. Rev. A* **2016**, *93*, 033840.
(54) Martínez-Martínez, L. A.; Ribeiro, R. F.; Campos-González-Angulo, J.; Yuen-Zhou, J. Can Ultrastrong Coupling Change Ground-State Chemical Reactions? *ACS Photonics* **2018**, *5*, 167–176.
(55) Galego, J.; Climent, C.; Garcia-Vidal, F. J.; Feist, J. Cavity Casimir-Polder Forces and Their Effects in Ground-State Chemical Reactivity. *Phys. Rev. X* **2019**, *9*, 021057.
(56) Pilar, P.; Bernardis, D. D.; Rabl, P. Thermodynamics of Ultrastrongly Coupled Light-Matter Systems. *Quantum* **2020**, *4*, 335.
(57) Li, T. E.; Nitzan, A.; Subotnik, J. E. On the Origin of Ground-State Vacuum-Field Catalysis: Equilibrium Consideration. *J. Chem. Phys.* **2020**, *152*, 234107.
(58) Dixon, I. M.; Rat, S.; Sournia-Saquet, A.; Molnár, G.; Salmon, L.; Bousseksou, A. On the Spin-State Dependence of Redox Potentials of Spin Crossover Complexes. *Inorg. Chem.* **2020**, *59*, 18402–18406.
(59) Malitson, I. H. Interspecimen Comparison of the Refractive Index of Fused Silica. *J. Opt. Soc. Am.* **1965**, *55*, 1205–1209.
(60) McPeak, K. M.; Jayanti, S. V.; Kress, S. J. P.; Meyer, S.; Iotti, S.; Rossinelli, A.; Norris, D. J. Plasmonic Films Can Easily Be Better: Rules and Recipes. *ACS Photonics* **2015**, *2*, 326–333.